Heliyon 5 (2019) e01764

Contents lists available at ScienceDirect

Heliyon

journal homepage: www.heliyon.com

Numerical investigation of obstacle's effect on the performance of proton-exchange membrane fuel cell: studying the shape of obstacles

A.A. Ebrahimzadeh, I. Khazaee *, A. Fasihfar

Faculty of Mechanical and Energy Engineering, Shahid Beheshti University, Tehran, Iran

ARTICLE INFO

Keyword:
Energy

ABSTRACT

Fuel cells are the technology through which chemical energy can be converted to electricity and heat. They perform the conversion with no contamination. Hence, they have become a significant source of clean power in today's modern life. That being said, it is really crucial that every source of power provides a high and stable amount of efficiency, and it should be considered when it comes to developing PEM fuel cell technology as well. One of the most important parameters in applying such fuel cells is the layout and dimensions of the flow field designed for the reactors on the bipolar plates of the fuel cell and its improvement. In the current research, for the best geometry dimension and arrangement of obstacles, four types of obstacle including triangular, cylindrical, square and trapezoidal are simulated. The obtained results show that the triangular obstacle has the best performance in terms of the produced current density and pressure drop. The results reveal that at the constant voltage of 0.6 V, the current density in the flow field with triangular and square obstacles is increased more than 80% in comparison to cylindrical and trapezoidal types. Finally, the fuel cell with triangular and square obstacles as the optimum flow field is designed, manufactured and tested.

1. Introduction

By and large, in the energy-oriented society we inhabit, the permanent exploitation of fossil fuels accounts for 82% of the total universal energy consumption which culminates in harmful effects on human being's lives. The more the human's population increases, the more fossil fuels should be burned to meet their electricity demand. The global warming crisis ensues from such activities. Not only does the fossil fuels consumption endanger people's health and threaten their environment, but the global fossil fuel reservoirs are tapering gradually so that they couldn't be used for the next generations. Hence, the world requires a source of power which possesses the following characteristic: low pollutant emissions, efficient energy production, and unlimited sources to meet the growing population of the world. For achieving these targets the fuel cells have been known as one of the most important technologies [1].

There are many ways for increasing PEMFC performance; one of them is designing new flow fields. There are many research activities in this field [2, 3, 4]. As well as, some new methods are presented [5, 6, 7,] that can be used for solving nonlinear equation that appears in PEMFC analysis.

It was founded that PEM fuel cell due to some advantages such as: low operation temperature, short start-up time and flexibility concerning dimensions and power are suitable for application in submarines [8]. The gas flow field is one of the most important components in PEM fuel cell. It should distribute the reactants on catalyst surface and removing the products of reaction. So far many patterns are introduce for gas floe field such as: parallel, serpentine, pinned, helicoid, etc. it. All of these patterns has some advantages and disadvantages. Several factors such as pressure drop, reactants distributing, controlling flow velocity, water removal, etc., are of vital importance and should be contemplated in designing the appropriate gas flow field [1]. Ferng et al. [9] numerically and experimentally investigated the effect of the flow channel patterns on PEM fuel cell performance. They studied two flow fields including: parallel and serpentine. They reported that performance of PEMFC with the serpentine flow channel is superior to that with the parallel one.

As another part of the research, the effect of channel depth on flow field with parallel and serpentine patterns was studied. The results reflected a significant impact when parallel channels had been applied. However, no impressive performance improvement was reported when serpentine channels were used. That being said, they didn't consider the other aspects of the channel. Scholta et al. [10] numerically studied

* Corresponding author.
E-mail address: Imankhazaee@yahoo.com (I. Khazaee).

https://doi.org/10.1016/j.heliyon.2019.e01764
Received 21 November 2018; Received in revised form 15 January 2019; Accepted 15 May 2019

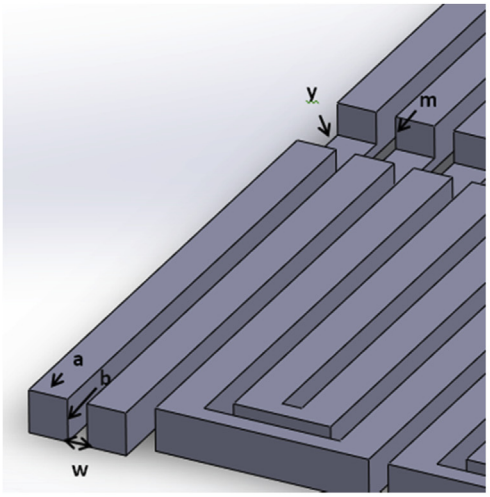

(a)

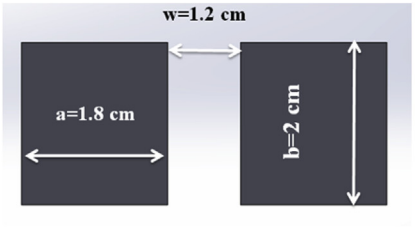

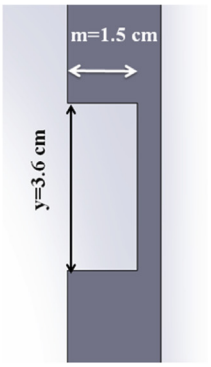

(b) (c)

Fig. 1. (a) Channel parameters, (b) channel geometrical size, (c) the depth and width of obstacle.

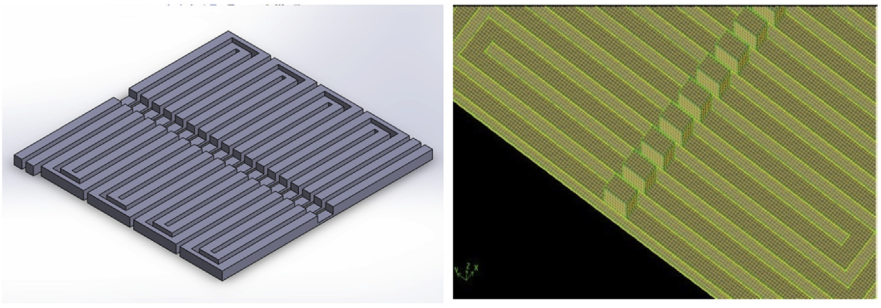

(a) (b)

Fig. 2. (a) The typical Gas flow field, (b) generated mesh in GAMBIT [27].

degree of parallelization in a parallel flow channel field. They investigated the effect of rib and width of channel on the polarization curve of a fuel cell. They reported narrow channels are more preferable for high current density, although, wider dimensions are more suitable at low current density. Yan et al. [11] used a three-dimensional numerical model to examine the effects of reductions of the outlet channel flow area on cell performance and local transport phenomena. They reported that the reductions of the outlet channel flow areas increase the reactant velocities in these regions, which enhance reactant transport, reactant utilization and liquid water removal. Therefore, the cell performance has been improved compared with the conventional serpentine flow field.

Lin et al. [12] and Seung et al. [13], presented an optimization method for a single serpentine fuel cell. They considered the height of flow channel as a variable factor. The optimized geometry showed 11.9 percent improvement on output power more than a cell with direct flow channels. Rahimi-Esbo et al. [14] using 3D numerical simulation investigated the results of reduction of channel at terminal part of flow field. The base flow field was considered a serpentine channel. They reported that water management will be improved by reducing the number of channels at the terminal part of the flow field. Liu et al. [15]

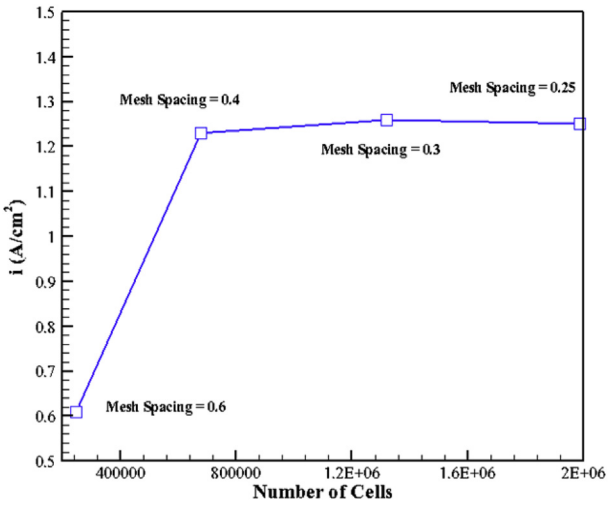

Fig. 3. Mesh independency study.

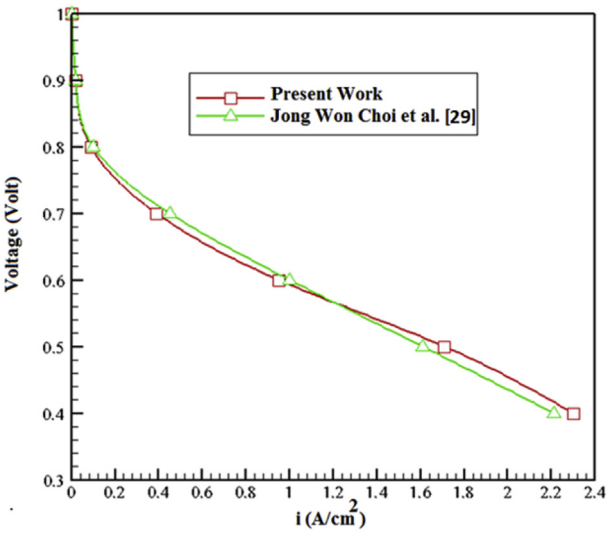

Fig. 4. Comparison of polarization curve of numerical simulation and experimental data of Won et al. [28].

Table 1
The input parameter for validation.

Temperature (K)	Gage pressure (bar)	Anode stoichiometry	Cathode stoichiometry	Active area (cm^2)
343	1	1.5	1.26	27.3

Other thermodynamics and physical parameters of PEM fuel cell for numerical simulation are presented in the literate [30].

experimentally investigate the effect of gas flow fields on fuel cell performance. Their results showed that the serpentine flow channel design is still favorable, giving the best single fuel cell performance amongst all the studied flow channel designs. They presented a novel symmetric serpentine flow field. They manufactured four fuel cell stacks, that each stack including four cells was assembled using different designs of serpentine flow channels. They reported that the presented novel gas flow field has the best performance compared to other. Khazaee and Sabadbafan [16] investigated the effect of inlet gas humidity and gas flow field direction in a 4-serpentine and a 1-serpentine flow field on performance of PEMFC. They presented that the cell performance at lower voltages augments with increasing humidity in the both cells and cell performance at all voltages increases in higher values of humidity percentage. Additionally, the parallel input and output direction is more appropriate for PEM fuel cell efficiency. Kahraman and Orhan [17] studied different gas flow fields and bipolar plates and discussed about their characteristics. Perng et al. [18] investigated the rectangular cross obstacle in the PEMFC flow field channel and figured out that the efficiency was improved. Han et al. [19] numerically and experimentally reviewed the effect of sinusoidal wall of channel on the efficiency of PEM fuel cell. Performance increasing in both numerical and experimental results has been presented in their report. Bilgili et al. [20] investigated the performance of PEMFC with considering obstacles at both cathode and anode channels. They reported obstacles heighten the gas density along the channel and higher cell voltages were achieved in high flow densities. Ghanbarian et al. [21] studied the effect of obstacles in channel on the performance of fuel cell. They showed that the performance of the cell enhanced by partial blockage of the flow channels in a parallel flow field. They used different types of obstacles such as square, semicircular and trapezoid. According to their report the trapezoid obstacles reflected higher increases in output power. Heidary and Kermani [22] studied the effect of heat exchange caused by partial obstacles in the channels of PEMFC flow field. Ashorynejad and Javaherdeh [23] employed Boltzmann method to investigate the effect of sinusoidal flow field on the

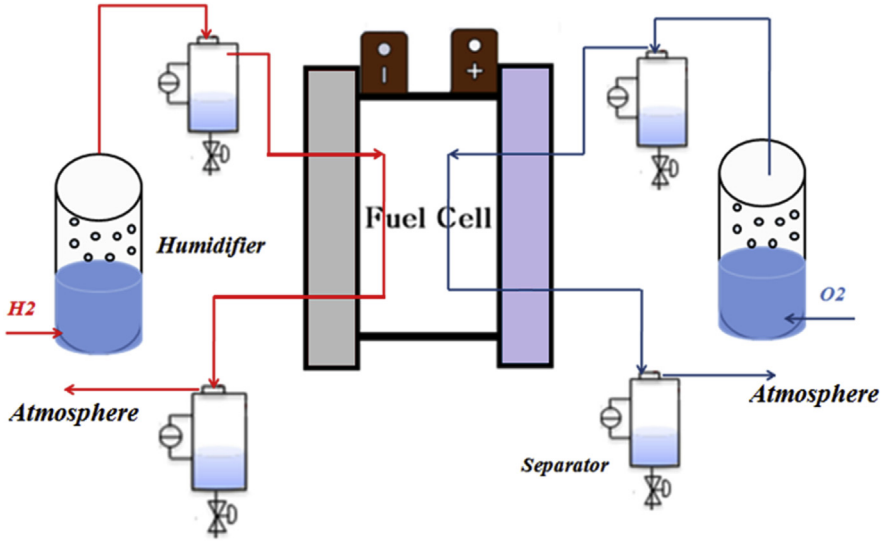

Fig. 5. Schematic of the proposed PEM fuel-cell test station.

Fig. 6. In-house test station with fuel cell in testing.

efficiency of fuel cell in a 2-D single-phase model. They considered only the cathode channel in the simulation. They concluded that the sinusoidal flow field augments the performance of the fuel cell with higher wavelength. Heidary et al. [24] numerically studied the effect of partial- or full-block placement along the flow channels of PEM fuel cells. They investigated the effect of obstacles number, its arrangement and placement in cathode and anode channels. Their results showed 30% improvement in performance for the sample with full obstacles of cathode with 5 obstacles. Heidary et al. [25] utilized obstacles in the flow field channel to ameliorate the efficiency of the fuel cell. As a result, an obstacle increases the gas penetration and it is specifically advantageous for the areas in which concentration drops.

In the literates, rarely can any comprehensive resource be found which has studied the obstacle in a serpentine flow field, pattern and its types. Most of them only studied the effect of square type obstacles on varied frequency domains or examined several obstacles in a steady state condition to compare the efficiencies. There is not any study which concentrates on calculating an optimum dimension and obstacle type. In our previous work, the geometrical dimension and arrangement of obstacle was optimized [26]. In the current research, for the first time in an optimum dimension and repetition pattern [26], four types of obstacles including square, triangular, cylindrical and trapezoid are investigated. Different parameters such as pressure drop, species distribution, temperature distribution and current density distribution are compared. By considering all parameters, it is found that the triangular obstacle is the best option for using in a fuel cell to increase the performance. Eventually, a fuel cell with triangular and square obstacles as optimum flow field is designed, manufactured and tested. The results of

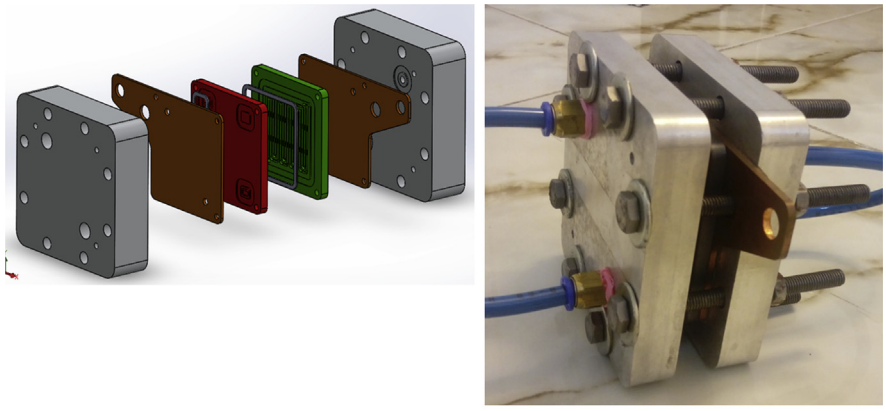

a) b)

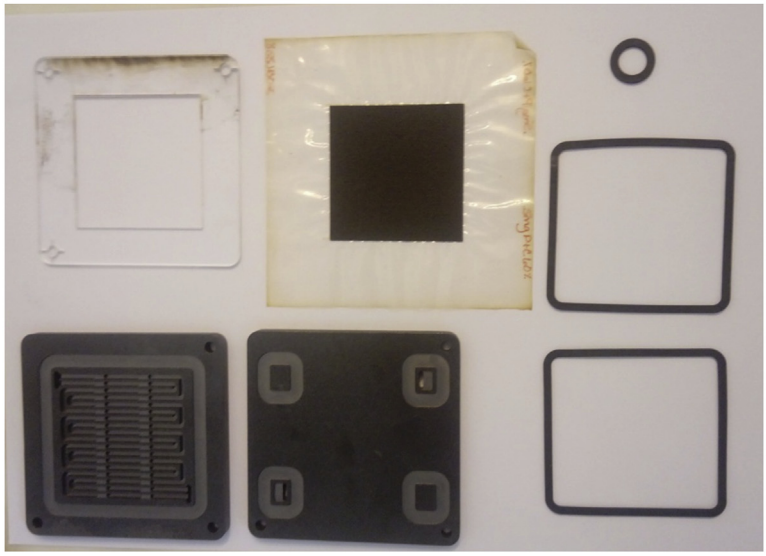

c)

Fig. 7. a)Design schematic b) Manufactured PEMFC c) Internal components.

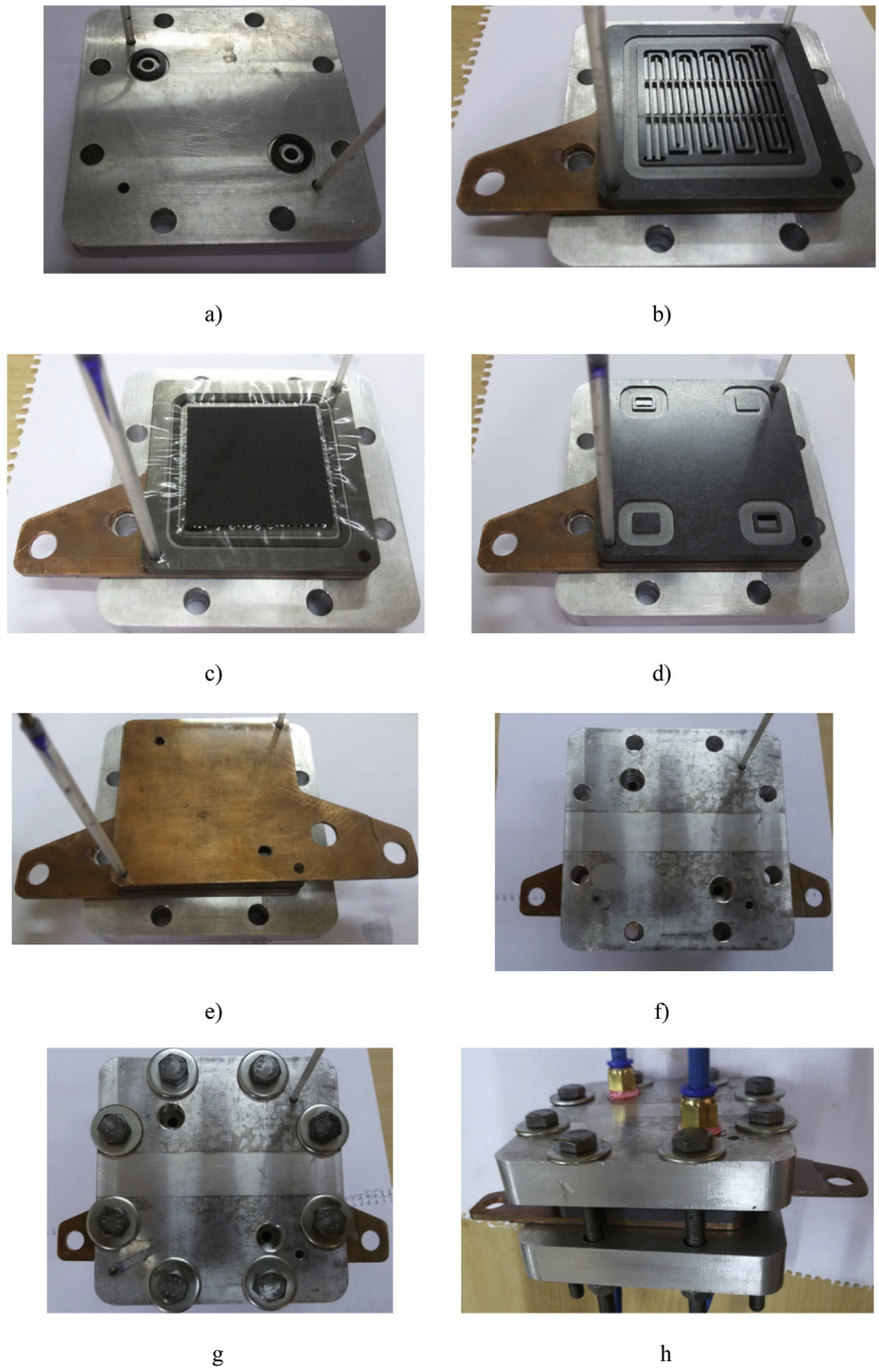

Fig. 8. Different steps of PEMFC fabricating.

experimental test verify the numerical results.

2. Model

The equation that should be solved in numerical simulation is presented in Eqs. (1), (2), (3), (4), (5), (6), (7), (8) [14].

$$\text{Mass (gas)} \quad \frac{\partial}{\partial t}\left(\varepsilon\rho^{(g)}\right)+\nabla.\left(\rho^{(g)}u^{(g)}\right)=S_{mass}-\dot{m}_{H_2O} \tag{1}$$

$$\text{Mass (liquid)} \quad \frac{\partial}{\partial t}\left(\varepsilon s\rho^{(l)}\right)+\nabla.\left(\rho^{(l)}u^{(l)}s\right)=\dot{m}_{H_2O} \tag{2}$$

$$\text{Momentum} \quad \frac{\partial}{\partial t}\left(\varepsilon\rho^{(g)}u^{(g)}\right)+\nabla.\left(\rho^{(g)}u^{(g)}u^{(g)}\right)=\nabla.\sigma-\frac{\mu^{(g)}}{k}u^{(g)} \tag{3}$$

$$\text{Energy} \quad \left(\rho C_P\right)_{eff}\frac{\partial}{\partial t}T+\nabla.\left(\left(\rho C_P\right)_{eff}u^{(g)}T\right)=\nabla.\left(k_{eff}\nabla T\right)+S_{temp} \tag{4}$$

$$\text{Species} \quad \frac{\partial}{\partial t}\left(\varepsilon\rho^{(g)}\omega_i^{(g)}\right)+\nabla.n_i^{(g)}=S_i \tag{5}$$

$$\text{Membrane water content} \quad \frac{\partial}{\partial t}\left(\frac{\rho^{(m)}M_{H_2O}\lambda}{M^{(m)}}\right)+\nabla.n_{H_2O}^{(m)}=S_\lambda \tag{6}$$

$$\text{Membrane potential} \quad \nabla.i^{(m)}=S_{pot} \tag{7}$$

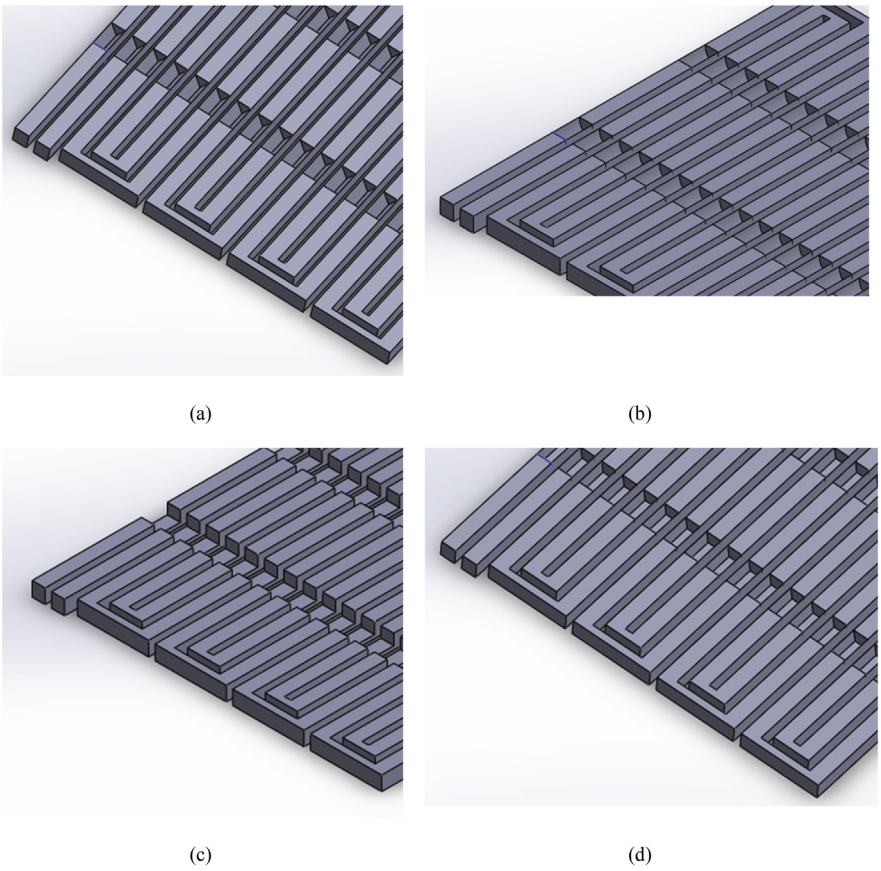

Fig. 9. Gas flow channel, (a) triangular, (b) cylindrical, (c) square and (d) trapezoid.

Solid potential $\nabla . i^{(s)} = -S_{pot}$ (8)

The source terms and parameters that appeared in the equation are explained with details in our previous paper [26] and are represented in Eqs. (9), (10), (11), (12), (13), (14), (15), (16), (17), (18), (19), (20), (21), (22), (23), (24), (25), and (26).

$$n_i^{(g)} = \rho^{(g)} u^{(g)} \omega_i^{(g)} - \rho^{(g)} D_{i,eff}^{(g)} \nabla \omega_i^{(g)} \quad (i = H_2, O_2, H_2O, N_2) \tag{9}$$

$$n_{H_2}^{(m)} = \frac{n_d M_{H_2O}}{F} i^{(m)} - \frac{\rho^{(g)}}{M^{(m)}} M_{H_2O} D_{H_2O,eff}^{(g)} \nabla \lambda \tag{10}$$

$$i^{(m)} = -\sigma_{eff}^{(m)} \nabla \varnothing^{(m)} \tag{11}$$

$$i^{(s)} = -\sigma_{eff}^{(s)} \nabla \varnothing^{(s)} \tag{12}$$

$$u^{(l)} = \begin{cases} u^{(g)} s - D^{(c)} \nabla s & (ff) \\ -D^{(c)} \nabla s & (gdl, cl) \end{cases} \tag{13}$$

$$\sigma = -P^{(g)} I + \mu^{(g)} \left[\nabla u^{(g)} + \left(\nabla u^{(g)} \right)^T \right] - \frac{2}{3} \mu^{(g)} \left(\nabla u^{(g)} \right) I \tag{14}$$

$$S_{mass} = \begin{cases} -\frac{M_{O_2} J_c}{4F} + \frac{M_{H_2O} J_c}{2F} - \nabla . n_{H_2O}^{(m)} & (cathode\ cl) \\ -\frac{M_{H_2O} J_a}{2F} - \nabla . n_{H_2O}^{(m)} & (anode\ cl) \\ 0 & (elsewhere) \end{cases} \tag{15}$$

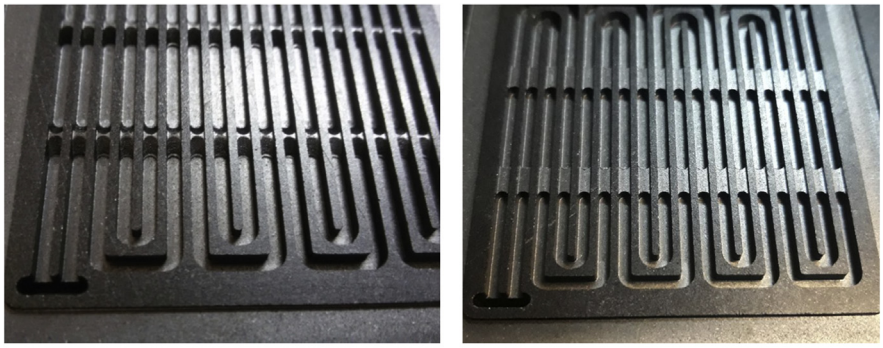

Fig. 10. The manufactured flow field a) Triangular b) rectangular.

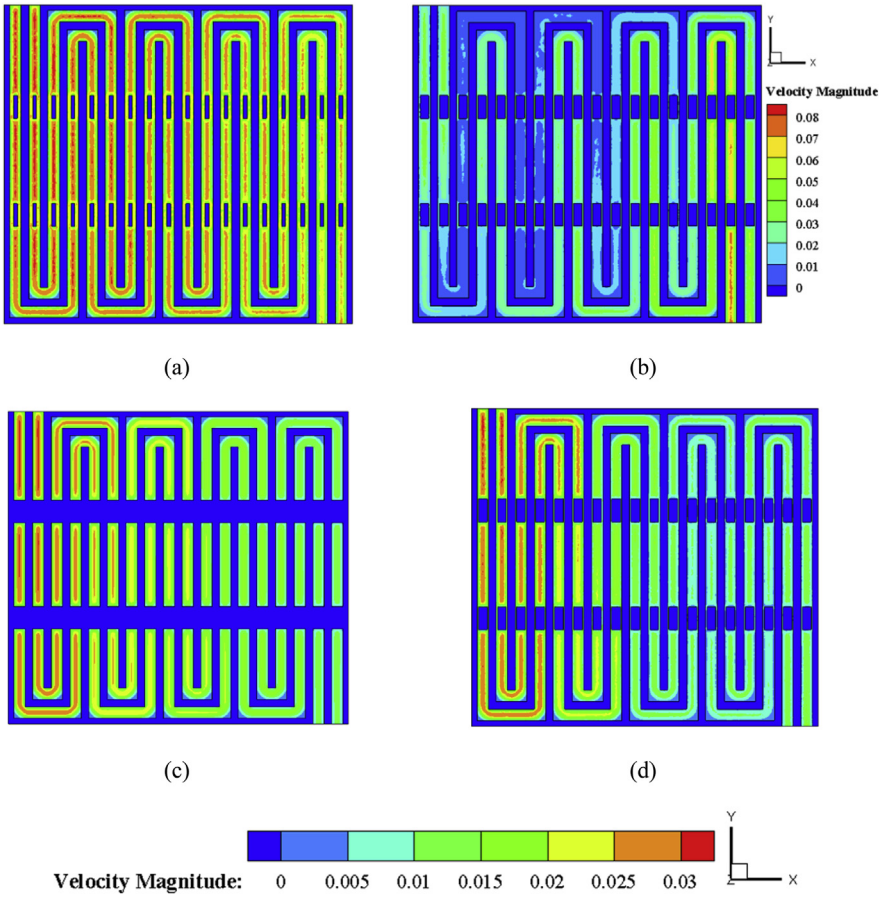

Fig. 11. Velocity diffusion at the centric surface of cathode channel for (a) triangular, (b) cylindrical, (c) square and (d) trapezoid obstacles at 0.8 V.

$$S_i = \begin{cases} -\dfrac{M_{O_2} J_c}{4F} & (O_2,\ cathode\ \ cl) \\ +\dfrac{M_{H_2O} J_c}{2F} - \nabla . n_{H_2O}^{(m)} - \dot{m}_{H_2O} & (H_2O,\ cathode\ \ cl) \\ -\nabla . n_{H_2O}^{(m)} - \dot{m}_{H_2O} & (H_2O,\ anode\ \ cl) \\ -\dot{m}_{H_2O} & (H_2O,\ gdl\,ff) \\ -\dfrac{M_{H_2O} J_a}{2F} & (H_2,\ anode\ cl) \\ 0 & (elsewhere) \end{cases} \tag{16}$$

$$S_\lambda = \begin{cases} -\nabla . n_{H_2O}^{(m)} & (cl) \\ 0 & (elsewhere) \end{cases} \tag{17}$$

$$S_{pot} = \begin{cases} -J_c & (cathode\ cl) \\ J_a & (anode\ cl) \\ 0 & (elsewhere) \end{cases} \tag{18}$$

$$\lambda = \begin{cases} 0.043 + 17.81a - 39.85a^2 + 36.0a^3 & a \le 1 \\ 14 + 1.4(a-1) & 1 < a \le 3 \end{cases} \tag{20}$$

$$a = \frac{P_{H_2O}^{(g)}}{P_{H_2O}^{sat}} + 2s \tag{21}$$

$$S_{temp} = \begin{cases} J_c\left(-T\dfrac{\partial E_{rev}}{\partial T} + |\eta_c| \right) + \sigma_{eff}^{(m)} \left(\nabla . \varnothing^{(m)}\right)^2 + \sigma_{eff}^{(s)} \left(\nabla . \varnothing^{(s)}\right)^2 + \dot{m}_{H_2O} H_{vap} & (cathode\ cl) \\ J_a \eta_a + \sigma_{eff}^{(m)} \left(\nabla . \varnothing^{(m)}\right)^2 + \sigma_{eff}^{(s)} \left(\nabla . \varnothing^{(s)}\right)^2 + \dot{m}_{H_2O} H_{vap} & (anode\ cl) \\ \sigma_{eff}^{(s)} \left(\nabla . \varnothing^{(s)}\right)^2 + \dot{m}_{H_2O} H_{vap} & (gdl) \\ \sigma_{eff}^{(m)} \left(\nabla . \varnothing^{(m)}\right)^2 & (m) \\ +\sigma_{eff}^{(s)} \left(\nabla . \varnothing^{(s)}\right)^2 & (ff,\ bp) \end{cases} \tag{19}$$

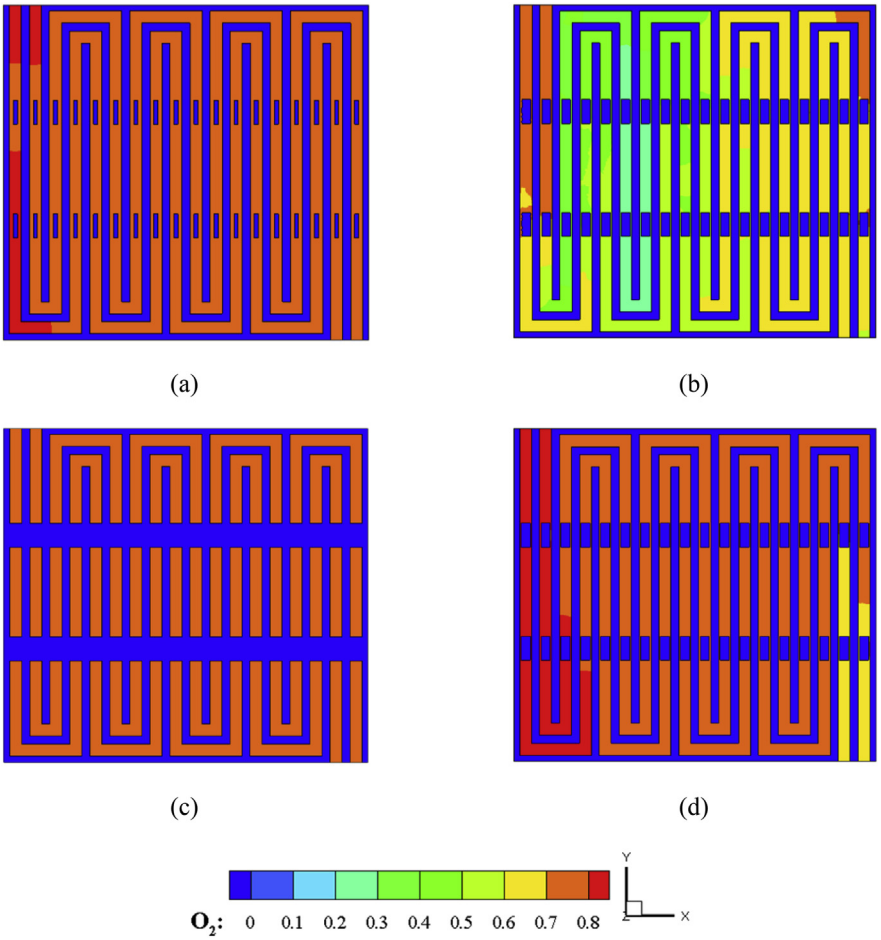

Fig. 12. Distribution of Oxygen concentration d at the centric surface of cathode gas flow channel for (a) triangular, (b) cylindrical, (c) square and (d) trapezoid obstacles at 0.8 V.

$$j_{an} = j_{an}^{ref}\left(\frac{C_{H_2}}{C_{H_2}^{ref}}\right)^{\gamma_{an}}\left(exp\left(\frac{\alpha_{an}F\eta_{an}}{RT}\right) - exp\left(-\frac{\alpha_{cat}F\eta_{an}}{RT}\right)\right) \quad (22)$$

$$j_{cat} = j_{cat}^{ref}\left(\frac{C_{O_2}}{C_{O_2}^{ref}}\right)^{\gamma_{cat}}\left(\exp\left(-\frac{\alpha_{cat}F\eta_{cat}}{RT}\right) - \exp\left(\frac{\alpha_{an}F\eta_{cat}}{RT}\right)\right) \quad (23)$$

$$\eta_{an} = -\varnothing_e \quad (24)$$

$$\eta_{cat} = V_{cell} - \varnothing_e - V_{oc} \quad (25)$$

$$V_{oc} = 1.23 - 9 \times 10^{-4}(T - 298) \quad (26)$$

Fig. 1a depicts both dimensional features of the channel. The geometrical parameters of obstacle are presented in Fig. 1b. Additionally, Fig. 2 shows the flow field and its mesh generated using GAMBIT 2.4. In order to investigate the mesh independency for a special geometry at a specified voltage; the variations of current density are investigated.

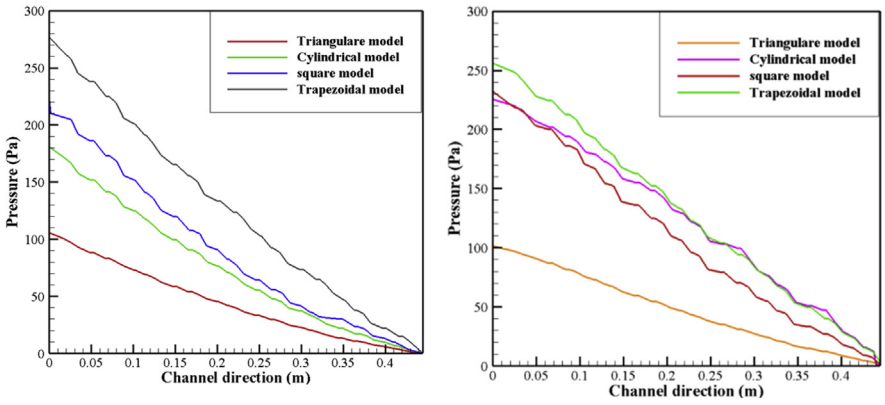

Fig. 13. (a) Variations of pressure along gas flow field channel at 0.4 V a) anode, (b) cathode.

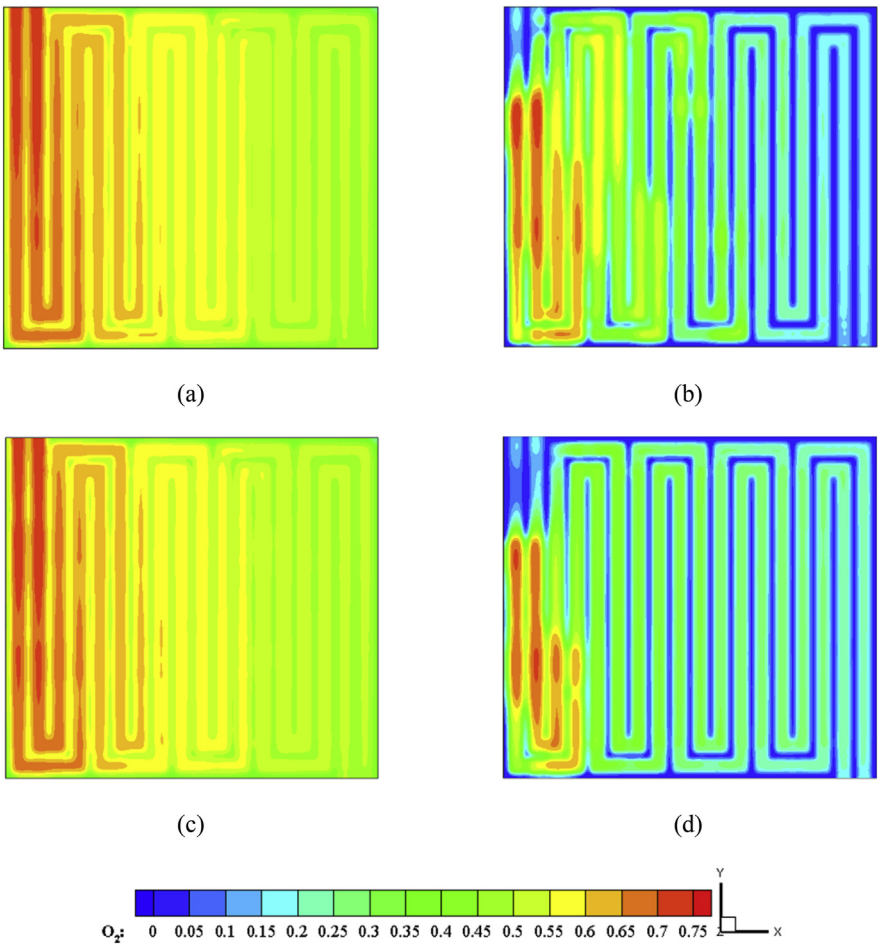

Fig. 14. Oxygen concentration distribution at interface of the catalyst layer and cathode gas diffusion layer for (a) triangular, (b) cylindrical, (c) square and (d) trapezoid obstacles at 0.8 V.

According to the difference between meshes spacing of 0.3 mm and 0.25 mm is approximately 0.8% the meshes spacing size of 0.3 mm and meshes number of 1400000 (Fig. 3) is selected for studying.

For certainty of accuracy of numerical results, it is compared and validated by experimental results of Jong Won Choi et al. [28]. Fig. 4 illustrates the comparison between the experimental data and numerical results. As it can be seen a good agreement is achieved.

In the current study, the simulation has been done by FLUENT ANSYS 16.2 [29]. The input parameters for comparing the results are listed in Table 1.

3. Experimental

Fig. 5 shows the schematic of the proposed design for a PEM fuel-cell. Liquid separators and bubble humidifier are used for separating the extra water and adding humid to inlet dry gas. The in-house test station that applied in this research can be seen in Fig. 6.

The Designed and manufactured and internal components of PEMFC including: MEA, flow fields and seals are presented in Fig. 7.

The different steps of fabricating are presented in Fig. 8.

4. Results and discussion

According to the selection of the best dimension and arrangement of obstacles that has been investigated in our previous work [26], in this manuscript, results obtained from obstacle type variation in terms of arrangement are studied. The square obstacle has been studied in the previous work for obtaining the best dimension and arrangement. In the following, the triangular (design a), cylindrical (design b), trapezoid (design d) and square (design c) are simulated and their results are presented in Figs. 9, 10, 11, 12, 13, 14, 15, and 16.

The manufactured flow field can be seen in Fig. 10 in very close distance.

The velocity dispersion at the middle of anode and cathode gas flow channel is shown in Fig. 11 at voltage of 0.8 V. It can be seen that the velocity decreases along the channel due to pressure drop and movement friction force. However, in this voltage, the fluid velocity is low due to low flow rate of reactants. It must be noted that in the cylindrical obstacle at the beginning of channel, the flow has very low velocity, where it might lead to high heat and undesirable performance of the fuel cell which is discussed later.

According to the velocity contour given in the previous section, the oxygen concentration distribution is shown in Fig. 12 at the centric surface of cathode flow channel at 0.8 V. As shown, the oxygen distribution has the highest value at the beginning of the path and traverses a decreasing trend along flow channel due to its participation in the chemical reaction. However, in the flow field with cylindrical obstacle, in the beginning of inlet, species concentration has lower value which is caused by the creation of a stop area and a low velocity of flow in this part.

Fig. 13 represents the pressure variation diagram along anode and cathode gas channels for voltage of 0.4 V. In the anode flow channel, the maximum pressure is 107, 182, 237 and 278Pa for obstacles (a), (b), (c) and (d) and in the cathode flow channel the maximum pressure is 103, 229, 236 and 261 which must be considered at fuel cell designing process. Results show that the triangular and square obstacles have lower

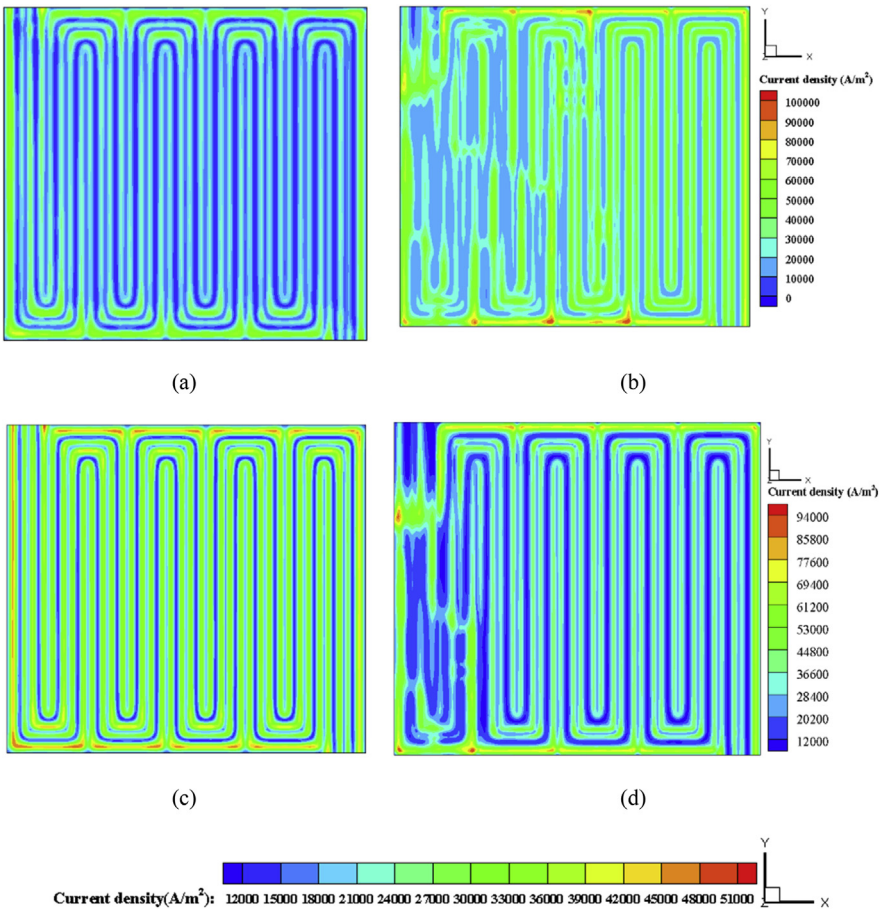

Fig. 15. Current density distribution in the interface of catalyst layer and cathode gas diffusion layer for (a) triangular, (b) cylindrical, (c) square and (d) trapezoid obstacles at 0.8 V voltage.

pressure drop over other obstacles and the trapezoid obstacle has the highest pressure drop.

In Fig. 14, oxygen concentration distribution at the interface of the catalyst layer and gas diffusion layer is shown at voltage of 0.4 and 0.8 V. At the lower voltage in the triangular and square obstacles, the oxygen concentration is the highest under the effect of cathode flow channel at the inlet part and decreases toward outlet. However, in the cylindrical obstacle, the oxygen concentration is higher in some parts of the flow channel. As a result, it would lead to inefficiency of the fuel which it can be seen at the produced current density.

The current density distribution in the interface of the catalyst layer and cathode GDL at voltage of 0.4 V is shown in Fig. 15. It can be seen that at the beginning areas of the flow channel with cylindrical and trapezoid obstacles, the produced current has heterogeneity and lower value than other flow field parts, since in these areas, the oxygen concentration is low and therefore, the reaction rate is low.

Temperature distribution at the centric surface of membrane is shown in Fig. 16 at voltage of 0.4 V. According to this figure and the above explanations, the temperature distribution of the triangular and square obstacle under the influence of gas flow channel has the lowest temperature at the inlet and by performing the chemical reactions and heat generation toward outlet, it has the highest temperature. At the same voltage, in the cylindrical obstacle, it is founded that in a place where the current reaches the stop state, the thermal aggregation occurs where this can also affect the undesirable performance of the fuel cell observed in current density.

In the obstacles location, due to of the compulsion to penetration a narrower space and more penetration of the species in the GDL, as a result of the reaction of most species, there is a higher heat which is called peak, and the path from the channel without an obstacle has lower temperature, which is called valley. It can be seen that the higher heat distribution in the cylindrical obstacle is made at the beginning of the flow channel than other obstacles, which is due to the stop state of species in this section.

Fig. 17 shows the polarization curve for different obstacles of square, triangular, trapezoid and cylindrical. At high voltage due to lower diffusing the reactant gasses a same performance is seen. It is observed that the current density values of the triangular and square obstacles are very close to each other and the produced current density of cylindrical and trapezoid obstacles is less than two other obstacles. According to the presented results and contours, the square and triangular obstacles have lower pressure drop and higher current density compare to other obstacles. Also, the pressure drop caused by the square obstacle is higher than that of triangular obstacle. As a result, it can be said that the triangular obstacle has the best performance on the simulated flow fields.

In Fig. 18 the numerical and experimental results are compared. As it can be seen a good agreement is achieved. In low voltage due a deviation is seen between numerical and experimental results. Difference between numerical and experimental results at higher current densities is meaningful. It can be related to two phase effects. There are many mechanisms for formation of liquid water that in numerical modeling cannot be modeled properly. In both experimental and numerical polarization curve, the flow field with triangular obstacles showed better performance.

5. Conclusion

In this paper, the effect of obstacles along the gas flow fields on the

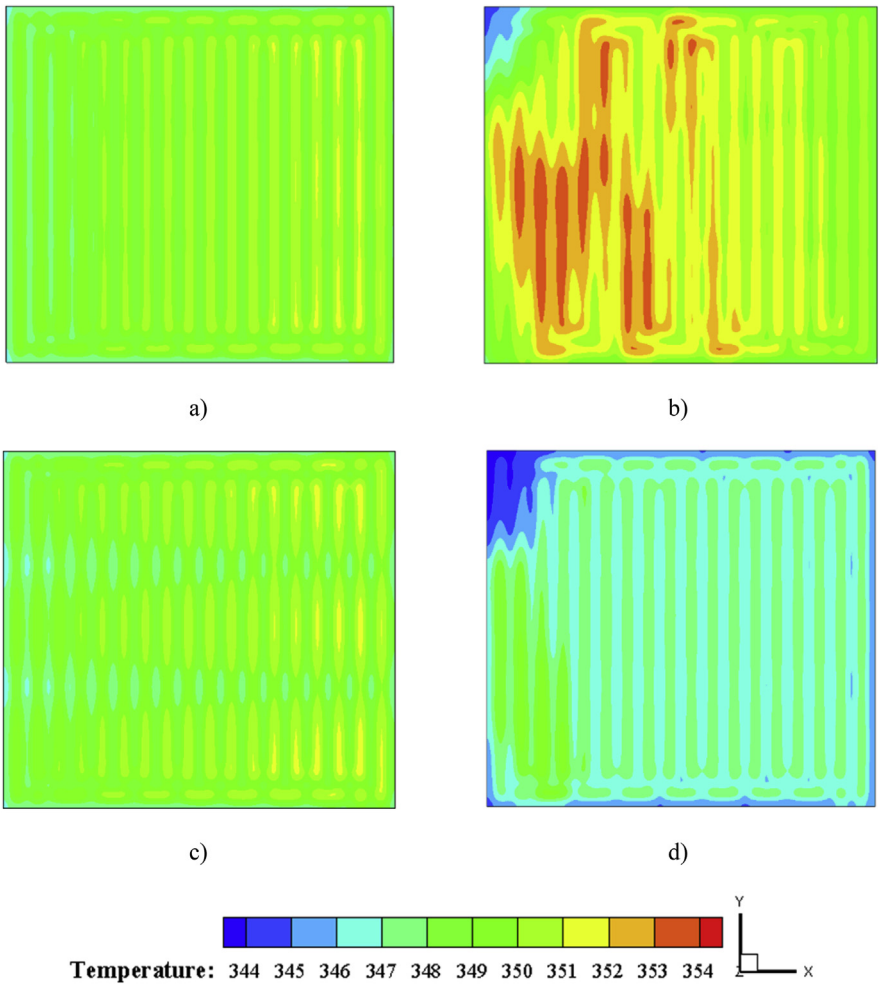

Fig. 16. Temperature distribution at the mid surface of the MEA for (a) triangular, (b) cylindrical, (c) square and (d) trapezoid obstacles at 0.8 V voltage.

efficiency of the fuel cell is studied. In our previous work, the best dimension and arrangement of obstacles is extracted [26]. In this paper the shape of obstacles and the optimal shape of it, is focused on. Four types of obstacles including triangular, cylindrical, square and trapezoid have been simulated and investigated. It has been observed that in cylindrical and trapezoidal obstacles in some areas of the flow field, the concentration of species has increased due to the formation of a stagnation area, which its impact on the produced current density can be seen. Therefore, the non-uniform current density is achieved. So, these two types of obstacles are not appropriate for using in a real PEMFC. The obtained results show that the triangular obstacle has the lowest pressure drop and highest species consumption rate and current density and therefore, it has been selected as the best type of obstacle. The square

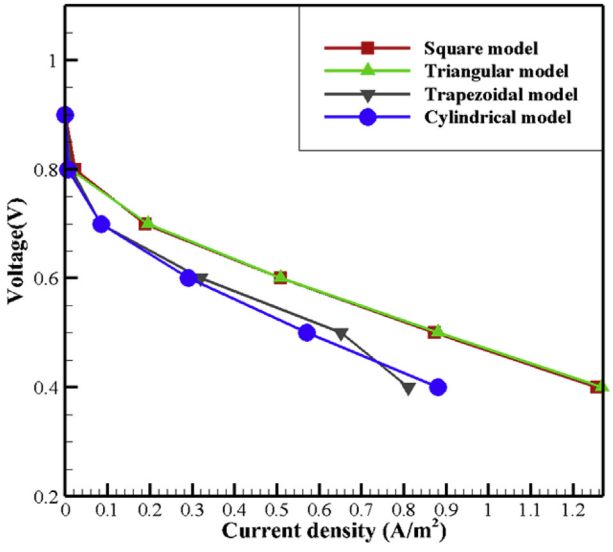

Fig. 17. Polarization curve for different obstacles of square, triangular, trapezoid and cylindrical along anode and cathode gas flow.

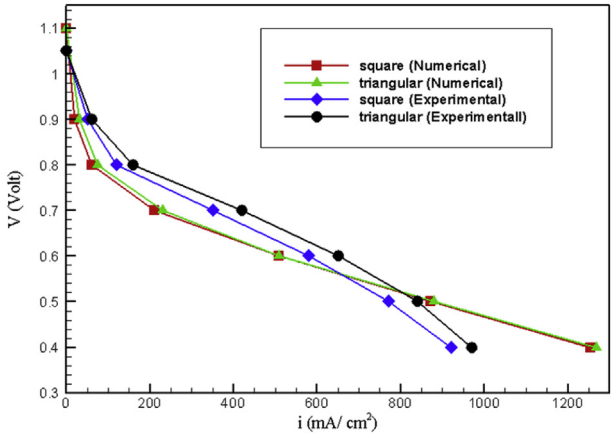

Fig. 18. Compare numerical and experimental results.

obstacle can be an appropriate selection, only due to its higher pressure drop in comparison to triangular obstacle. The cylindrical obstacle has the worst performance in current generation due to undesirable distribution of species, temperature and etc. The results reveal that at the constant voltage of 0.6 V, the current density in flow field with triangular and square obstacle is increased more than 80% compare to cylindrical and trapezoidal. At the last part of manuscript, according to numerical results a PEMFC with this optimal dimensions and obstacle type is designed, manufactured and tested. As well as the experimental results are compared with numerical results and verified the numerical results.

Declarations

Author contribution statement

A. A. Ebrahimzadeh & I. Khazaee: Conceived and designed the experiments; Performed the experiments; Analyzed and interpreted the data; Contributed reagents, materials, analysis tools or data; Wrote the paper.

A. Fasihfar: Analyzed and interpreted the data; Contributed reagents, materials, analysis tools or data; Wrote the paper.

Funding statement

This research did not receive any specific grant from funding agencies in the public, commercial, or not-for-profit sectors.

Competing interest statement

The authors declare no conflict of interest.

Additional information

No additional information is available for this paper.

References

[1] F. Barbir, PEM Fuel Cells: Theory and Practice, Academic Press, 2013.
[2] Y. Kerkoub, A. Benzaoui, F. Haddad, K. YasminaZiari, Channel to rib width ratio influence with various flow field designs on performance of PEM fuel cell, Energy Convers. Manag. 174 (2018) 260–275.
[3] A. Baricci, R. Mereu, M. Messaggi, M. Zago, F. Inzoli, A. Casalegno, Application of computational fluid dynamics to the analysis of geometrical features in PEM fuel cells flow fields with the aid of impedance spectroscopy, Appl. Energy 205 (2017) 670–682.
[4] M. ZiauddinChowdhury, Y. ErkanAkansu, Novel convergent-divergent serpentine flow fields effect on PEM fuel cell performance, Int. J. Hydrogen Energy 42 (2017) 25686–25694.
[5] M. Sheikholeslami, Haq Rizwan-ul, Shafee Ahmad, Zhixiong Li, Heat transfer behavior of nanoparticle enhanced PCM solidification through an enclosure with V shaped fins, Int. J. Heat Mass Transf. 130 (2019) 1322–1342.
[6] M. Sheikholeslami, New computational approach for exergy and entropy analysis of nanofluid under the impact of Lorentz force through a porous media, Comput. Methods Appl. Mech. Eng. 344 (2019) 319–333.
[7] M. Sheikholeslami, Numerical approach for MHD Al2O3-water nanofluid transportation inside a permeable medium using innovative computer method, Comput. Methods Appl. Mech. Eng. 344 (2019) 306–318.
[8] A. Psoma, G. Sattler, Fuel cell systems for submarines: from the first idea to serial production, J. Power Sources 106 (1–2) (2002) 381–383.
[9] FerngYuh-Ming, SuAyandLu Shao-Ming, Experiment and simulation investigations for effects of flow channel patterns on the PEMFC performance, Int. J. Energy Res. 32 (2008) 12–23.
[10] J. Scholta, G. Escher, W. Zhang, L. Kü ppers, L. Jö rissen, W. Lehnert, Investigation on the influence of channel geometries on PEMFC performance, J. Power Sources 155 (2006) 66–71.
[11] Y. Wei-Mon, L. Hung-Yi, C. Po-Chiao, W. Xiao-Dong, Effects of serpentineflowfieldwithoutletchannel contraction on cell performance of proton exchange membrane fuel cells, J. Power Sources (2008) 174–180.
[12] L. Lin, Z. XinXin, F. Hu Ting, W. Xiao-Dong, Optimization of a serpentine flow field with variable channel heights and widths for PEM fuel cells, Sci. China Technol. Sci. 53 (2010) 453–460.
[13] C. Kap-Seung, K. Hyung-Man, M. Sung-Mo, Numerical studies on the geometrical characterization of serpentine flow-field for efficient PEMFC, Int. J. Hydrogen Energy 36 (2011) 1613–1627.
[14] M. Rahimi-Esbo, A.A. Ranjbar, A. Ramiar, E. Alizadeh, Improving PEMFC performance using a novel flow field, Int. J. Hydrogen Energy 37 (2016) 2490–2497.
[15] H. Liu, P. Li, D. Juarez-Robles, K. Wang, A. Hernandez-Guerrero, Experimental study and comparison of various designs of gas flow fields to PEM fuel cells and cell stack performance, Frontiers Energy Res 2 (2014) 1–8.
[16] I. khazaee, H. Sabadbafan, Effect of humidity content and direction of the flow of reactant gases on water management in the 4-serpentine and 1-serpentine flow channel in a PEM (proton exchange membrane) fuel cell, Energy 101 (2016) 252–265.
[17] H. Kahraman, Mehmet F. Orhan, Flow field bipolar plates in a proton exchange membrane fuel cell: analysis& modeling, Energy Convers. Manag. 133 (2017) 363–384.
[18] S.W. Perng, H.W. Wu, Effects of internal flow modification on the cell performance enhancement of a PEM fuel cell, J. Power Sources 175 (2008) 806–816.
[19] S.H. Han, N.H. Choi, Y.D. Choi, Simulation and experimental analysis on the performance of PEM fuel cell by the wave-like surface design at the cathode channel, Int. J. Hydrogen Energy 37 (2012) 1613–1627.
[20] M. Bilgili, M. Bosomoiu, G. Tsotridis, Gas flow field with obstacles for PEM fuel cells at different operating conditions, Int. J. Hydrogen Energy 40 (2015) 2303–2311.
[21] A. Ghanbarian, M.J. Kermani, Enhancement of PEM fuel cell performance by flow channel indentation, Energy Convers. Manag. 110 (2016) 356–366.
[22] H. Heidary, M.J. Kermani, Performance enhancement of fuel cells using bipolar plate duct indentations, effect of nano-particles on forced convection in sinusoidal-wall channel, Int. J. Hydrogen Energy 38 (2013) 5485–5496.
[23] H.R. Ashorynejad, K. Javaherdeh, Investigation of a waveform cathode channel on the performance of aPEM fuel cell by means of a pore-scale multi-component lattice Boltzmann method, J. Taiwan Inst. Chem. Eng. (2016) 1–11.
[24] H. Heidary, M.J. Kermani, B. Dabir, Influences of bipolar plate channel blockages on PEM fuel cell performances, Energy Convers. Manag. 124 (2016) 51–60.
[25] H. Heidary, M.J. Kermani, S.G. Advani, Ajay K. Prasad, Experimental investigation of in-line and staggered blockages in parallel flow field channels of PEM fuel cells, Int. J. Hydrogen Energy 41 (2016) 688–693.
[26] A.A. Ebrahimzadeh, I. Khazaee, A. Fasihfar, Numerical investigation of dimensions and arrangement of obstacle on the performance of PEM fuel cell, Heliyon 4 (2018), e00974.
[27] http://citeseerx.ist.psu.edu/viewdoc/download?.
[28] W.Ch. Jong, H. Yong-Sheen, W.C. Suk, S.K. Min, Experimental study on enhancing the fuel efficiency of an anodic dead-end mode polymer electrolyte membrane fuel cell by oscillating the hydrogen, Int. J. Hydrogen Energy 35 (2010) 12469–12479.
[29] https://www.sharcnet.ca/Software/Fluent16/pdf/fuelcells/flfuelcells.pdf.
[30] M. Ghasemi, A. Ramiar, A.A. Ranjbar, S.M. Rahgoshay, A numerical study on thermal analysis and cooling flow field's effect on PEMFC performance, Int. J. Hydrogen Energy (2018) 1–19.